Electrochromic Performances of Poly(Azure A) Films from Digital Video-Electrochemistry (DVEC)

Journal of The Electrochemical Society, 2020 **167** 106514
1945-7111/2020/167(10)/106514/9/$40.00 © 2020 The Electrochemical Society ("ECS"). Published on behalf of ECS by IOP Publishing Limited

Electrochromic Performances of Poly(Azure A) Films from Digital Video-Electrochemistry (DVEC)

Esteban Guillén, Jerónimo Agrisuelas,[z] José J. García-Jareño, and Francisco Vicente[*,z]

Departament de Química Física, Universitat de València, Burjassot, 46100 València, Spain

Poly(Azure A) (PAA) films doped with sodium dodecyl sulfate (SDS) were grown on transparent indium tin oxide (ITO) glass substrates by cyclic voltammetry. The electrochromism of PAA was investigated by digital video-electrochemistry (DVEC). DVEC consists of the acquisition of sequential digital images during the electro-stimulated changes of PAA color. The evolution of red, green, and blue (R, G, B) colors intensity (I) of analyzed pixels provides enough sensitivity to detect changes of some nmol cm^{-2} of electroactive centers. Besides, the different time evolution of these color intensities can serve to discern among different electroactive centers activated in the polymer. For the first time, contrast, coloration efficiency, and bleaching times of PAA are calculated by DVEC. The coloration efficiencies were between 15–25 cm^2 mC^{-1} with short response times for the bleaching process between 2.9 and 5.5 s. PAA has good electrochromic performances to be used in electrochromic devices. Our present work provides an important insight into the design principles for a practical application of DVEC to characterize electrochromic devices in light-controlled conditions allowing us to find the best performances of these materials.
 [DOI: 10.1149/1945-7111/ab9e3b]

Manuscript submitted May 15, 2020; revised manuscript received June 11, 2020. Published June 29, 2020.

Electrochromic devices have attracted significant attention in the last few decades due to the reversible switching of the optical transmittance upon the electrochemical reactions of the electroactive material. Many existing chemical systems are intrinsically electrochromic, such as inorganic compounds, transition metal oxides, or organic molecules.[1–4] Conjugated organic polymers prove very attractive in the fast-growing electrochromic materials since they combine mechanical flexibility, ease in color-tuning, low-cost scalability, and processing.[5]

Organic polymers based on phenothiazines, a class of heterocyclic organic compounds, are often used to obtain modified electrodes in a simple form on several types of substrates.[6–10] The heterocycle consists of sp^3-hybridized electron-rich nitrogen and sulfur atoms, and it can form ordered structures between polymer chains via interactions of the side chains.[11] However, the electrochemical characteristics are less known than other N-based polymers such as polyaniline or polypyrrole.[12,13] Despite this, many of them have been used within a wide range of technological applications, such as sensors,[14–17] organic light-emitting diodes,[18] batteries,[19] corrosion protection,[20,21] photochemistry,[22] supercapacitors,[23] electrochemical catalysis.[24]

The conducting and redox polymer poly(Azure A) (PAA) is easily synthetized by electrooxidation of the monomer dye (*N*,*N*′-dimethylphenothiazin-5-ium-3,7-diamine).[25] PAA shows a complex redox activity since two different electroactive centers in the polymeric chain can be reduced or oxidized.[26,27] On the one hand, the heterocycle of the phenothiazine ring, which is not altered during the polymerization process providing color to the polymer.[28,29] On the other hand, the new bonds generated during the oxidative polymerization to link the monomers have a similar structure as in polyaniline films.[27,30] Figure 1a shows the schematic structure of the assumed electroactive centers in the PAA polymer. The oxidation and reduction of these electroactive centers involve the electrochromic changes.[30] PAA films exhibit a wide absorption band between 450 nm and 750 nm (peak maximum at ∼630 nm) within a low potential range of [0.1,−0.3] V changing between a dark blue film (oxidized) and a pale blue film (reduced).[31]

The inactivation of PAA in certain circumstances entails a constant search for new synthetic routes to improve the operational aspects of this kind of polymers.[32] In this way, aqueous anionic micellar solutions are being recently used to electrosynthesize different polymers.[33–35] Sodium dodecyl sulfate (SDS) is an anionic surfactant consisting of a polar head with a long hydrophobic tail (Fig. 1b). SDS enhances the electron transfer between the electrode surface and electroactive species[36,37] and provides an excellent environment to dissolve azine monomers above the critical micellar concentration.[38] Besides, SDS doping modifies the elasticity and mechanical properties of films[39] and the selectivity of the anion/cation insertion inside films.[40] PAA films polymerized in SDS solutions have shown enhancing electrochemical and sensor properties.[9,41]

In electrochromism studies, spectroscopic techniques usually cover the visible region of the electromagnetic radiation and digital images are used to show statically blanched or colored stated of materials.[42–46] Digital video-electrochemistry (DVEC) consists of recording digital videos of the electrode surface during induced electrochromic changes.[47] The color of one pixel in a digital image is a combination of red (R), green (G) and blue (B) colors intensity and supply transmitted color information about 650 nm, 510 nm, and 475 nm wavelengths, respectively. In particular, green color is close to the most sensitive average wavelength for the human eye (555 nm) under daylight conditions.[43,48] In any digital image of an 8-bit color resolution, each color is quantized in 256 intensity levels where 255 is the fully bright color, and 0 means the color is turned off. This allows reaching 16777216 (256 × 256 × 256) combinations or colors. Thus, DVEC rises as a complementary and alternative technique to traditional spectroscopy because any image captured by a digital camera collects information with enough resolution in the visible region. The key advantage of DVEC is the analysis of spatiotemporal color changes on the complete electrode surface without working in extremely dark conditions or with transparent electrodes during the electrochemical transitions.[47,49–52]

As far as we know, few studies focus on electrochromic performances of electrosynthesized phenothiazine-based polymers.[33–55] In particular, no study addresses the electrochromic performances of PAA despite the electrochromic properties of this kind of polymers are known.[26,30,56] Besides, this investigation is also relevant for showing the advantages of DVEC in the electrochromism field. Thus, the aims of this work are, on the one hand, to explore the RGB electrochromic switching of PAA on ITO electrodes and, on the other hand, to prove DVEC as a suitable technique for the characterization of quality and performance of electrochromic devices. This was conducted by the acquisition of 30 digital images per second during the electrically induced color changes of PAA by cyclic voltammetry, potential step chronoamperometry, and electrochemical impedance spectroscopy.

*Electrochemical Society Member.
[z]E-mail: jeronimo.agrisuelas@uv.es; francisco.vicente@uv.es

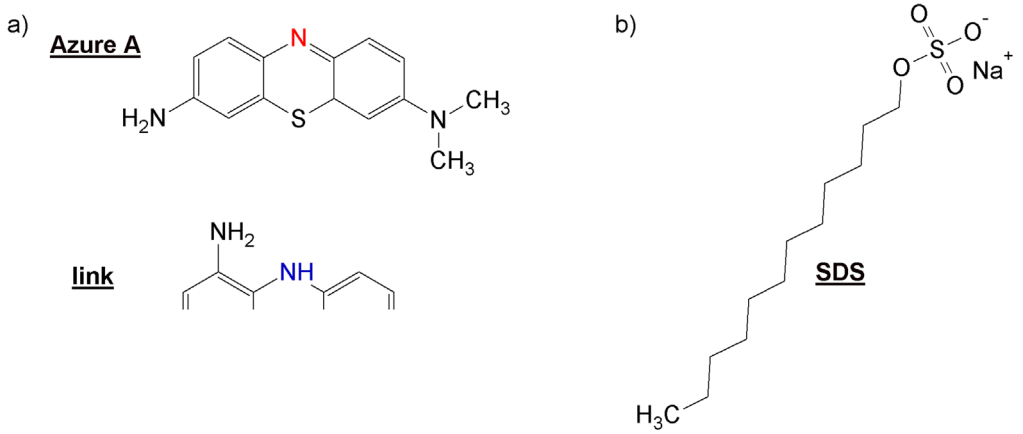

Figure 1. (a) The assumed structural configuration of the electroactive nitrogen in the heterocycle of the phenothiazine rings (red) and the electroactive polyaniline-type link (blue) in PAA.[30,54] (b) The molecular structure of sodium dodecyl sulfate (SDS).

Experimental

Electrosynthesis.—The polymerization solution was 0.2 mg ml^{-1} of Azure A (Sigma Aldrich), 0.1 M HCl (Scharlau, reagent grade 37%), and 20 mM SDS (Sigma, reagent grade 95%) with pH 1.7. The SDS concentration assures the formation of micelles.[57] PAA films were synthesized by cyclic voltammetry between −0.25 V and 1.1 V (starting potential 0.5 V) at 10 mV s^{-1} for 20 times in a typical three-electrode cell. ITO (resistivity of 30 Ω cm^{-1}) electrodes with a 1 × 1 cm^2 electroactive area were cleaned with acetone and Milli-Q water previously to polymer deposition and used as working electrodes. A platinum mesh was used as the counter electrode. A silver wire was the quasireference electrode for the polymerization with equivalent results than a commercial one. After deposition, the modified electrodes were cleaned with enough Milli-Q water to eliminate residual monomers and stored before use as working electrodes. All solutions were freshly prepared with distilled and deionized water (MilliQ-plus, Millipore, resistivity 18.2 MΩ cm) and chemicals were used as received. Like in similar conditions,[9,30] the polymerization of PAA with SDS on the ITO electrode by cyclic voltammetry starts when the potential arrives at 0.8 V followed by the irreversible anodic peak at about 0.935 V corresponding with the oxidative radicalization of monomers to form the polymer.[25] At about 0.1 V, the peaks system has been assigned to the electrochemical reactions of the PAA.

Electrochromic characterization.—Electrochemical experiments were performed with a PAR 273A potentiostat/galvanostat. For the electrochromic characterization, Ag|AgCl|KCl$_{(sat)}$ was the reference electrode, which was separated with a membrane from the electrolyte solution by a bridge tube with a porous glass frit (CoralPor) supplied by BioLogic. Cyclic voltammetry was performed over the potential range of 0.5 and −0.6 V at scan rates of 10, 20, 40, 60 80 and 100 mV s^{-1} with 60 s of stabilization at 0.5 V. Chronoamperometry was performed over the potential range of 0.5 and −0.6 V with 60 s of stabilization at 0.5 V and a potential step of 10 s. Electrochemical impedance spectroscopy was performed between 10 KHz and 10 mHz with 5 points per decade and a potential perturbation amplitude of 20 mV *rms*. The parameters of the equivalent circuit elements were obtained from a nonlinear square fitting executed using a home-made software based on the Levenberg-Marquardt algorithm.

The electrolyte solution consisted in 0.1 M acetate buffer (pH 2.9, 3.4, 4.3 or 5.8) and 0.45 M $NaNO_3$. Acetic acid (Scharlau, synthetic grade 99.5%), sodium acetate (Sigma-Aldrich for molecular biology, anhydrous >99.5%), and $NaNO_3$ (Scharlau, synthetic grade 99.5%). The electrochemical cell was a high-transmittance glass cell (Hellma, OG quality) with a 25 × 25 mm optical path length illuminated with a white LED strip (PowerLED, 6500K). PAA electrochromism was characterized by DVEC using a digital endoscope camera (Pontensic, B01059-P-NT) capturing 1280 × 720 pixels RGB digital videos at 30 frames per second (fps).

As explained elsewhere,[47,49] digital videos were recorded during the electrochemical characterizations and all frames were extracted. Cropped images of the area of interest for each of the frames were decomposed into three color arrays of RGB intensities by a home-made software. From a practical point of view due to a large number of analyzed areas and pixels, the mean color intensities for each color array ($\bar{I}_R$, $\bar{I}_G$ and $\bar{I}_B$) were calculated as:

$$\bar{I} = \frac{\sum_{i=1}^{n_p} I_i}{n_p} \quad [1]$$

where I_i is the color intensity of the pixel i and n_p is the total number of pixels in the analyzed area. For data interpretation, raw $\bar{I}$ data were appropriately smoothed using a Savitzky–Golay filter unless otherwise specified.

Results and Discussion

Cyclic voltammetry.—DVEC analysis was conducted to understand the RGB electrochromic behavior of PAA films between 0.5 and −0.6 V at 10 mV s^{-1} using cyclic voltammetry (Fig. 2). The electrode shows a pale greyish blue color at 0.5 V due to the planar aromatic structure of phenothiazine rings because the heterocycle is oxidized. At −0.6 V, the reduction of the heterocycle folds the phenothiazine molecular structure bleaching the polymers.[58] Figure 2a shows the evolution of $\bar{I}$ of the analyzed area during the coloring-to-bleaching transition. The color change is quantified by the full-switch contrast (C) as:

$$C_{R,G,B} = \bar{I}^b - \bar{I}^c \quad [2]$$

where $\bar{I}^b$ and $\bar{I}^c$ refer to the mean color intensity of the coloring and bleaching state of the film for each color. The contrast of the red (C_R) is the highest with an increment of 32 units between both PAA states. C_G and C_B show values of 28 and 14 intensity units, respectively. These values correspond to 12.4%, 10.9%, and 5.5% of the total intensity interval (256 intensity units), respectively. Therefore, DVCE allows us to extract valuable information about our electrochromic electrode.

The color change rate, $d\bar{I}/dt$, was calculated since this kinetic magnitude is analog to the rate of flow of electric charge.[49,59] In agreement with spectrophotometry data,[31] $d\bar{I}/dt$ peaks match with current peaks and shoulders recorded in the voltammetry. The proposed electrochemical mechanism for PAA consists of four reaction steps with the formation of intermediate species (PAA*) where anions and protons exchange to keep the electroneutrality of film.[60] On the one hand, the electrochemical reaction involving the

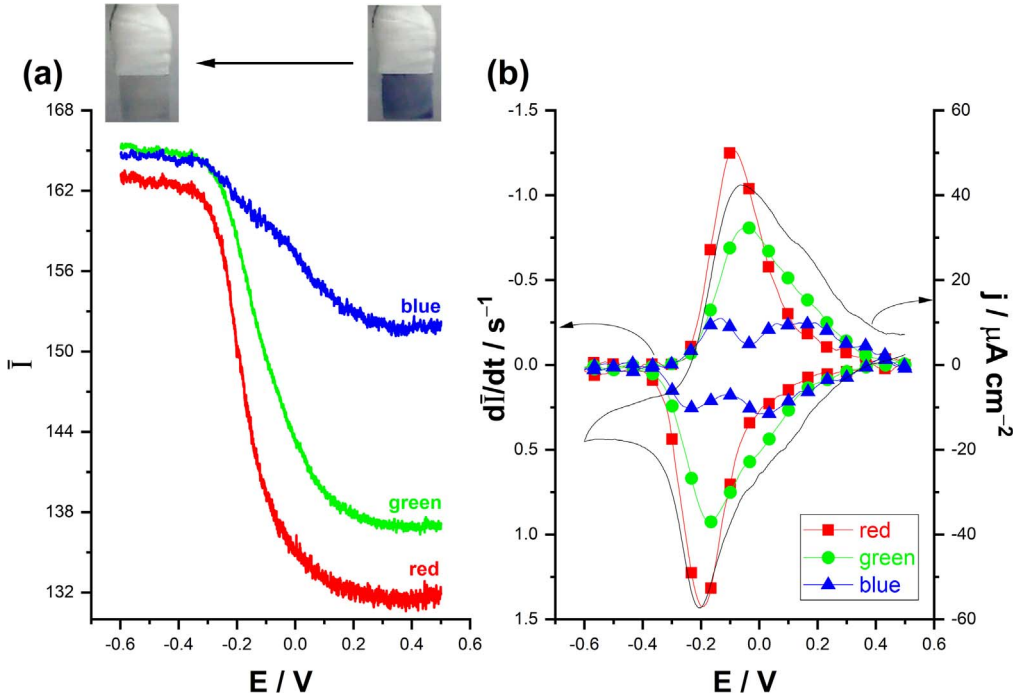

Figure 2. (a) Raw R, G, and B color mean intensity and (b) dī/dt and the current response of PAA film during the cyclic voltammetry of PAA film in 0.1 M acetate buffer (pH 5.8) and 0.45 M $NaNO_3$ with a scan rate of 10 mV s^{-1}.

links takes place at potentials around 0.1 V with the following reactions steps:

$$[(PAA^{ox}_{link})^+, A^-] + e^- \leftrightarrows PAA^*_{link} + A^- \quad [3]$$

$$PAA^*_{link} + H^+ + e^- \leftrightarrows PAA^{red}_{link} \quad [4]$$

Around 0.15 V, the current shows an overlapped electrochemical couple, $d\bar{I}_G/dt$ shows a shoulder due to small green color changes and $d\bar{I}_B/dt$ shows a well-defined electrochromic couple with an apparent formal potential ($E^{0\prime}$) at 0.075 V calculated as the mean between the oxidation and reduction potential peaks of $d\bar{I}_B/dt$.

On the other hand, the phenothiazine ring of PAA shows electroactivity around −0.1 V with the following reactions steps:

$$[(PAA^{ox}_{ring})^+, A^-] + e^- \leftrightarrows PAA^*_{ring} + A^- \quad [5]$$

$$PAA^*_{ring} + H^+ + e^- \leftrightarrows PAA^{red}_{ring} \quad [6]$$

At these potentials, $d\bar{I}_R/dt$, $d\bar{I}_G/dt$ and $d\bar{I}_B/dt$ show evident electrochromic couples with $E^{0\prime} = -0.14$ V, −0.1 V, and −0.18 V, respectively, synchronized with the electrochemical couple at $E^{0\prime} = -0.135$ V (Fig. 2b). As the color of PAA is principally due to the phenothiazine rings, the folding/unfolding of these rings involves changes in the three colors. Beyond −0.4 V, PAA bleaching is stable since $d\bar{I}/dt$ of the three colors is close to 0 and the observed current density could be attributed to the hydrogen evolution catalyzed by PAA film.[32] Thus, the potential window where electrochromic changes take place is well defined between 0.4 V and −0.4 V. DVEC provides complementary results as spectrophotometry analysis.[31]

As can be seen, $d\bar{I}_R/dt$ and $d\bar{I}_B/dt$ gives precise information about correlating electrochromic changes with electrochemical reactions. Taking as reference previous spectrophotometry data, $d\bar{I}_R/dt$ could only depend on phenothiazine color changes since synchronizes with the electrochemical couple at −0.14 V in agreement with absorbance changes at 495 nm.[31] Blue color agrees with absorbance at 590 nm associated with the electrochromic changes of links and phenothiazines inside PAA films synthesized in KNO_3. However, unlike previous spectrophotometry data, $d\bar{I}_B/dt$ obtained from DVEC shows two well-separated electrochromic couples, which can be associated with each of the electroactive centers during the potentiodynamic scan. Dodecyl sulfate ions inserted inside the film could be the origin of this significant result.

Scan rate.—Figure 3a shows the cyclic RGB voltammograms obtained for PAA films by cycling the potential between 0.5 and –0.6 V at the potential scan rates from 10 to 100 mV s^{-1}. The voltammograms show well $d\bar{I}_R/dt$ and $d\bar{I}_G/dt$ electrochromic couples for all scan rates. $d\bar{I}_B/dt$ oxidation peaks are lost at the fastest scan rates. As shown in Fig. 3b both the anodic and cathodic peaks of $d\bar{I}/dt$ increase linearly with increasing scan rate, with good regression coefficients and symmetry (Table I) indicating surface-confined electrochromic processes for both electroactive centers of the PAA. $d\bar{I}_R/dt$ shows the highest peaks due to the fast changes of red color. Figure 3c shows the evolution of contrast (Eq. 2) with the scan rate. The red color shows the highest values at all scan rates, but like the green color, the contrast decreases as the scan rate increases. C_B remains almost constant at all scan rates.

pH effect.—As in other N-based polymers,[61,62] protons are essential in the electrochemical reactions of PAA as proposed in Eqs. 4 and 6. Figure 4 shows the effect of pH on the electrochromic

Table I. Parameters of linear fittings from Fig. 3b.

Color	$(d\bar{I}/dt)_{peak}$	Slope (mV^{-1})	R^2
Red	I_a	−67	0.999
	I_c	66	0.996
Green	II_a	−42	0.990
	II_c	45	0.996
Blue	III_a	−13	0.984
	III_c	20	0.998
	IV_a	−19	0.999
	IV_c	21	0.995

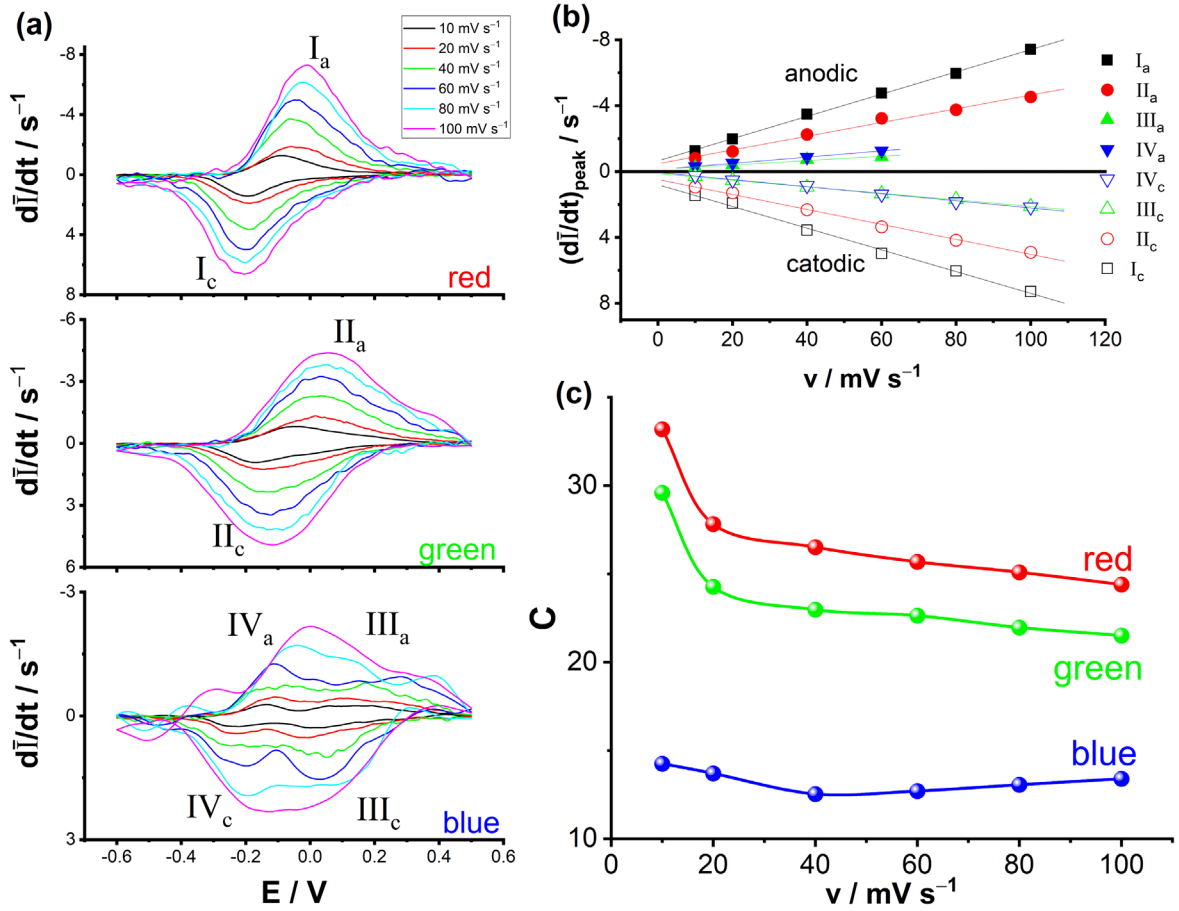

Figure 3. (a) $d\bar{I}/dt$ of PAA film during the cyclic voltammetry of PAA film in 0.1 M acetate buffer (pH 5.8) and 0.45 M $NaNO_3$ with a scan rate between 10–100 mV s^{-1}. (b) Variation of anodic and cathodic $(d\bar{I}/dt)_{peak}$ of R, G and B colors with scan rate for PAA films where solid lines are the linear fittings. (c) Variation of contrast (Eq. 2) for R, G, and B color with scan rate.

changes in the PAA between 2.9 and 5.8. As seen, potentials of $d\bar{I}/dt$ peaks (E_p) show a shift towards negative potential with increasing pH indicating proton-coupled electrons transfer reactions during the PAA electrochromic changes. The number of protons involved in the electrochromic process was assessed from the slope of E_p vs pH plots of Fig. 4a. For a Nernstian process at 298 K, peak potential will vary by $59.1\frac{m}{n}$ mV pH^{-1} for an m-proton/n-electron redox process. Slopes of $91\frac{m}{n}$ mV pH^{-1} (peak II_a) and 100 mV pH^{-1} (peak II_c) and of 86 mV pH^{-1} (peak I_a) and 72 mV pH^{-1} (peak I_c) suggest the $2H^+$:$1e^-$ proportion for green and red color changes. Blue color shows slopes around 60 mV pH^{-1} for the peaks III suggesting $1H^+$:$1e^-$ proportion, while 31–43 mV pH^{-1} (anodic-cathodic) for the peaks IV suggests $1H^+$:$2e^-$ proportion.

These pH dependences could be due to the complex interplay between the multi-protic polymeric nature of PAA electrochromic centers with changing pH. Besides, dodecyl sulfate anions fixed inside the PAA during the polymerization could also alter the proposed PAA mechanism by repulsing, to some extent, anions from the electrolyte increasing the participation of protons to keep the electroneutrality during the electrochemical reactions. Figure 4b shows that the PAA contrast proves maximum at pH 3.4 with 19% of change for the red, 16% for the green, and 7% for the blue color.

Potential step chronoamperometry.—Figure 5a compares the response time of RGB to the bleaching electrochromic process. The colored state was achieved at 0.5 V during 60 s, later potential steps between 0.4 and −0.6 V were applied during 10 s. Contrast evolution (ΔC) with the elapsed time (t) for one electrochromic switch can be represented, and fitted, to the following exponential increases function[63,64]:

$$\Delta C_{R,G,B} = \Delta C^{max}_{R,G,B}(1 - e^{-t/\tau_{R,G,B}}) \quad [7]$$

where $\Delta C^{max}_{R,G,B}$ is the full-switch contrast obtained for a potential step, and $\tau_{R,G,B}$ is the time constant for each color. $\Delta C^{max}_{R,G,B}$ is equal to $\Delta C_{R,G,B}$ (Eq. 2) when the potential step reaches the bleaching state. This allows clarifying the quantitative difference of electrochromic changes speed and the electrochromic switching mechanism of PAA. However, all electrochromic curves of Fig. 5a do not fit exactly with Eq. 7.

As examples, Fig. 5b shows fittings with ΔC_B at the potential step of −0.1 V (top graph) and ΔC_R at the potential step of −0.5 V (bottom graph). Both colors are chosen because they could be associated with one of the two electroactive centers in these experimental conditions. On the one hand, ΔC_B at −0.1 V fits well with Eq. 7 since the blue electrochromic changes only depend on the electrochemical reaction of links as expected by voltammetry results. On the other hand, the red electrochromic changes seem to be associated only with the phenothiazine rings, as commented above. However, the fitting of ΔC_R at −0.5 V fits well when two overlapped bleaching processes are considered. The latter also occurs for all ΔC_G signals and for ΔC_B at potentials steps beyond −0.1 V where links and rings are reduced simultaneously.

Overlapping exponential equations based on Eq. 7 have been used to understand the electrochromic response at 650 nm of polyaniline films concluding two overlapped optical responses.[64] However, they could not compare with an electrochromic response due to one electrochemical process. Our results show both situations confirming that two electrochemical reactions can affect the same color. This finding allows us to propose this mathematical procedure as a simple

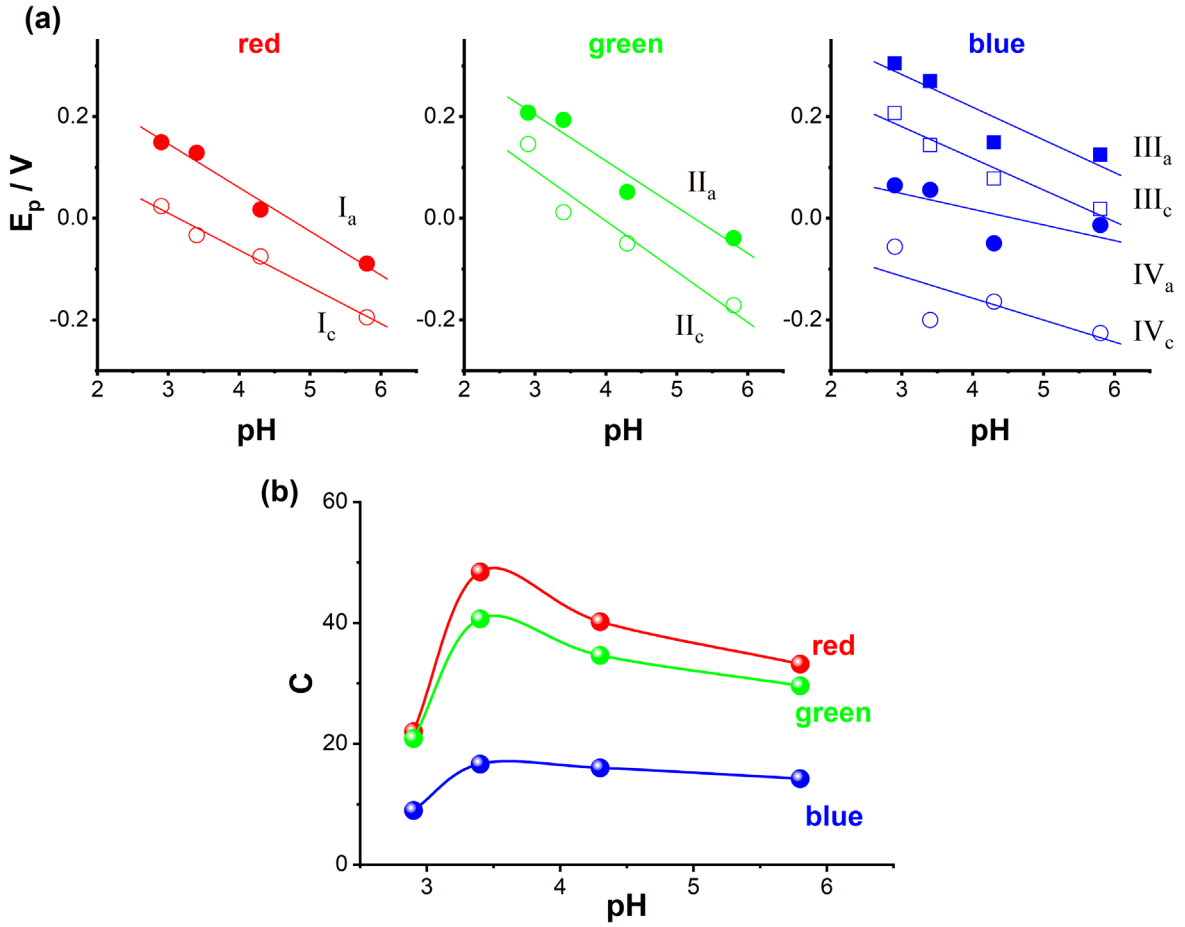

Figure 4. (a) Variation of E_p of $(d\bar{I}/dt/)_{peak}$ of R, G and B colors (Fig. 3a) with pH for PAA in 0.1 M acetate buffer (pH 2.9, 3.4, 4.3 and 5.8) and 0.45 M $NaNO_3$ with a scan rate of 10 mV s^{-1} where solid lines are the linear fittings. (b) Variation of contrast (Eq. 2) for R, G, and B color with pH.

test to predict the number of electrochemical reactions involving one optical change. The number of overlapping exponential functions needed to obtain good correlation coefficients provides the number of electrochemical processes involved with the chromic change.

Color switching.—As calculated with other spectroscopic techniques, the response time of electrochromic materials can be measured by DVEC because obtaining short switching time is important in materials predisposed to be used in electrochromic devices.[43] Bleaching times to achieve 95% of $\Delta C^{max}_{R,G,B}$ ($t^{R,G,B}_{95}$) were calculated from raw data since, as discussed above, the electrochromic processes are affected by electrochemical reactions of both rings and links. The best blue and green bleachings were observed at –0.2 V with $t^{B}_{95} = 5.5$ s and at –0.3 V with $t^{G}_{95} = 3.6$ s, respectively. At –0.4 V, the red bleaching shows the best t^{R}_{95} with 2.9 s. PAA shows a good time response for the red bleaching because the oxidation or reduction of the adsorbed film on the electrode surface would depend on electron hopping between the ITO surface and the electroactive centers. Similar t_{95} were obtained at the other pH.

Bleaching times of some chemically synthetized polymers with phenothiazine groups were about 3 s at 597 nm (t_{100}),[65] 3 s at 1056 nm (t_{100}),[66] 4 s at 522 nm (t_{90})[67] and electrochemically synthetized polymers with phenothiazine groups are 0.5 s at 500 nm and 0.85 s at 610 nm (t_{100}),[68] 1.8 s at 610 nm and 0.6 s 580 nm (t_{100}),[69] 0.98 s at 970 nm (t_{90}).[70] These results suggest that PAA shows enough promising electrochromic characteristic to be used in colored-to-transmissive electrochromic devices.

Coloration efficiency.—One of the most important criteria for a full assessment of electrochromic materials is the coloration efficiency.[43] A good electrochromic material would exhibit a large color change with a small amount of charge. By DVEC, the coloration efficiency can be calculated as the ratio between $\Delta C^{max}_{R,G,B}$ for the three colors and the injected charge (ΔQ) per unit electrode area:

$$CE_{R,G,B} = \frac{\Delta C^{max}_{R,G,B}}{\Delta Q} \quad [8]$$

Figure 5c shows the coloration efficiency evolution depending on the pH and potential steps. The best coloration efficiencies were reached at pH 2.9 for the three colors, concretely, at potential steps between 0.1 and −0.1 V with values around 15–25 cm^2 mC^{-1}. That can be due to the simultaneous participation of both electroactive centers since their electrochemical potentials are displaced to more positive values (Fig. 4a). As the distance between the electrochemical potentials of both centers increases when pH is less and less acidic, the coloration efficiency is slightly reduced.

Despite this, an interesting result is regarded when the evolution of the coloration efficiency is analyzed at pH 5.8. In the steps to positive potentials where links are electroactive, CE_G shows values around 15 cm^2 mC^{-1}. In the steps to negative potentials, CE_R reaches similar values and CE_G decays when links and ring reactions take place. From a practical point of view, electrochromic devices based on PAA films could have two different operational conditions: preferent green color passing with potential steps between 0.5 V and 0.1 V or preferent red color passing with potential pulses between −0.2 V and −0.4 V controlling the pH of the electrolyte solution.

Coloration efficiencies from DVEC and electrochemical impedance spectroscopy.—The electrochemical impedance analysis

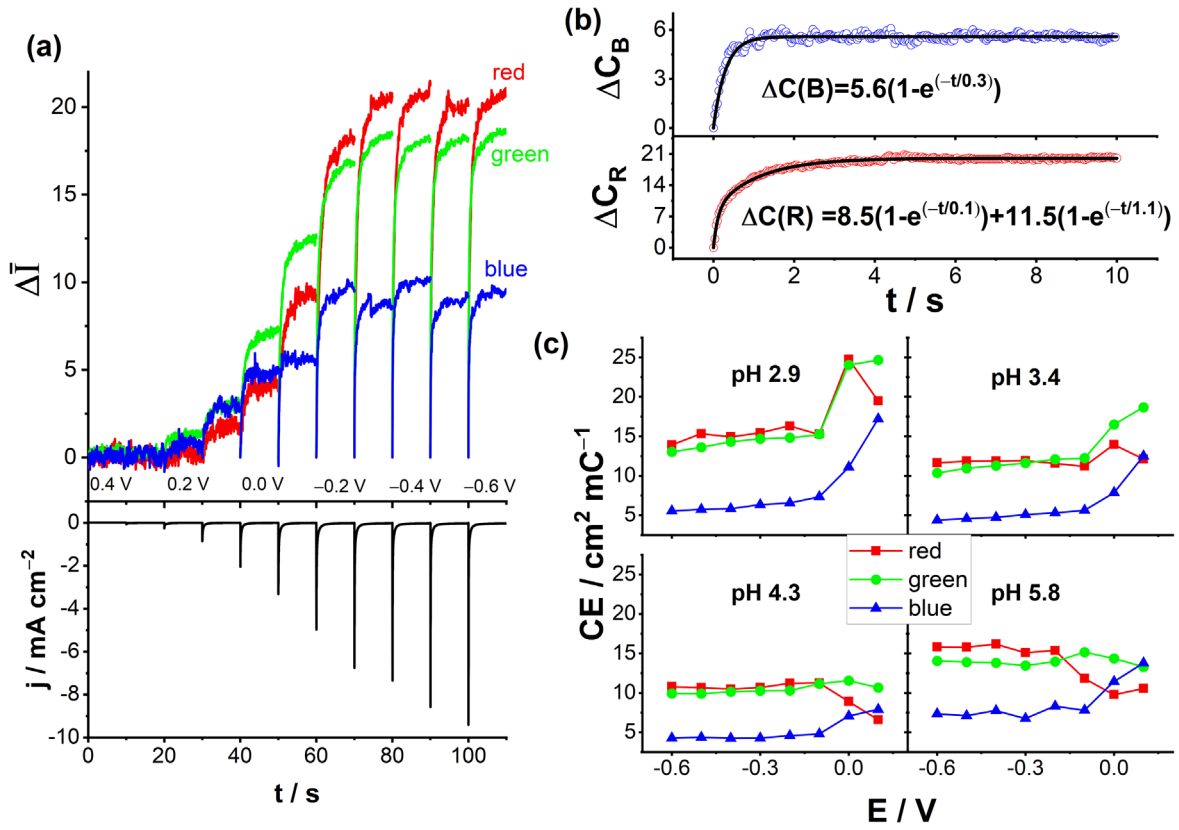

Figure 5. (a) Raw R, G, and B mean color intensity change and current change when PAA film is switching between 0.5 V and 0.4–0.6 V in 0.1 M acetate buffer (pH 5.8) and 0.45 M $NaNO_3$. (b) ΔC_B for the potential step of −0.1 V and ΔC_R for the potential step of −0.5 V with fittings to the exponential rise function (Eq. 7). (c) Color efficiency for R, G, and B (Eq. 8) depending on potential pulse and pH.

was performed to provide information about the electrode resistance, the capacitive behavior, and the associated electrochromic changes. The Nyquist plot from 10 KHz to 10 mHz at pH 3 (Fig. 6) exhibits a depressed semicircle in the high-frequency region related to a fast electron transfer followed by an inclined straight line in the low-frequency region due to the slow electron transfer.[27,71] All impedance spectra fit well with the modified Randles circuit typically used to explain the electric behavior of thin films.[27,72] The uncompensated resistance of the electrochemical cell (R_u) and the double-layer capacitance of the active layer at the polymer|solution interface (C_{dl}) were obtained from the high frequencies impedance data and fixed to 42 Ω cm^2 and 12 μF cm^{-2}, respectively. Both the expected values for a 1 cm^2 ITO electrode.[31]

The charge-transfer resistance of the active layer (R_{ct}) and the constant phase element of the charge-transfer capacitance (CPE_{ct}) describe the fast processes. R_{ct} reaches the lowest value (1.4 kΩ cm^2 in Table II) at 0.1 V near to the $E^{0\prime}$ of PAA at this pH (0.135 V) calculated from potential peaks of the control voltammogram. CPE_{ct} proves close to an ideal capacitor for the fast transfer processes since the obtained exponents (n_{ct}) was 0.83 ± 0.03 for all potentials studied. As the potential is more negative, the fast processes decrease the activity, and, in consequence, CPE_{ct} decreases. TL is the transmission line related to the slow electrochemical processes. R_{tl} and C_{tl} are the resistance and capacitance associated with the transmission line with values around 20 kΩ cm^2 and 0.5 mC cm^{-2}, respectively. C_{lt} increases together with the increasing electrochemical participation of rings at more negative potentials.

Figure 7a shows the color changes at 10 mHz where the best coloration efficiencies are expected considering the results of Fig. 3c. The wave amplitude of red, green, and blue provide information about the potentials where the optical changes are more intense. The red color increases the amplitude of color change as the potential is increasingly negative like the green color but with a larger wave amplitude. The blue color decreases the wave amplitude until 0.15 V, then it increases again as the potentials are more negatives.

From impedance data, CE_{EIS} is calculated considering that the capacitance (C) of the film is:

$$C = \frac{1}{j\omega Z} \quad [9]$$

where Z is the impedance, $j = \sqrt{-1}$ and $\omega = 2\pi f$ where f is the perturbation frequency. The real and imaginary parts of the faradaic capacitance (C_{Re} and C_{Im}, respectively) at a given frequency are:

$$C_{Re} = \frac{-Z_{Im}}{((Z_{Re} - R_u)^2 + Z_{Im}^2)\omega} \quad [10]$$

$$C_{Im} = \frac{Z_{Re} - R_u}{((Z_{Re} - R_u)^2 + Z_{Im}^2)\omega} \quad [11]$$

and the modulus of C can be calculated as:

$$|C| = \sqrt{C_{Re}^2 + C_{Im}^2} = \frac{\Delta Q}{\Delta E} \quad [12]$$

Therefore,

$$CE_{R,G,B}^{EIS} = \frac{\Delta \bar{I}_{R,G,B}}{\Delta Q} = \frac{\Delta \bar{I}_{R,G,B}/\Delta E}{\Delta Q/\Delta E} \quad [13]$$

where $\Delta \bar{I}_{R,G,B}$ is the color change amplitude calculated as $\bar{I}_{R,G,B}^{max} - \bar{I}_{R,G,B}^{min}$ from the sinusoidal curve (Fig. 7a) and ΔE is known from the potential perturbation amplitude (0.02 V *rms* = 0.02 × $\sqrt{2}$ V) for a given frequency perturbation and color.

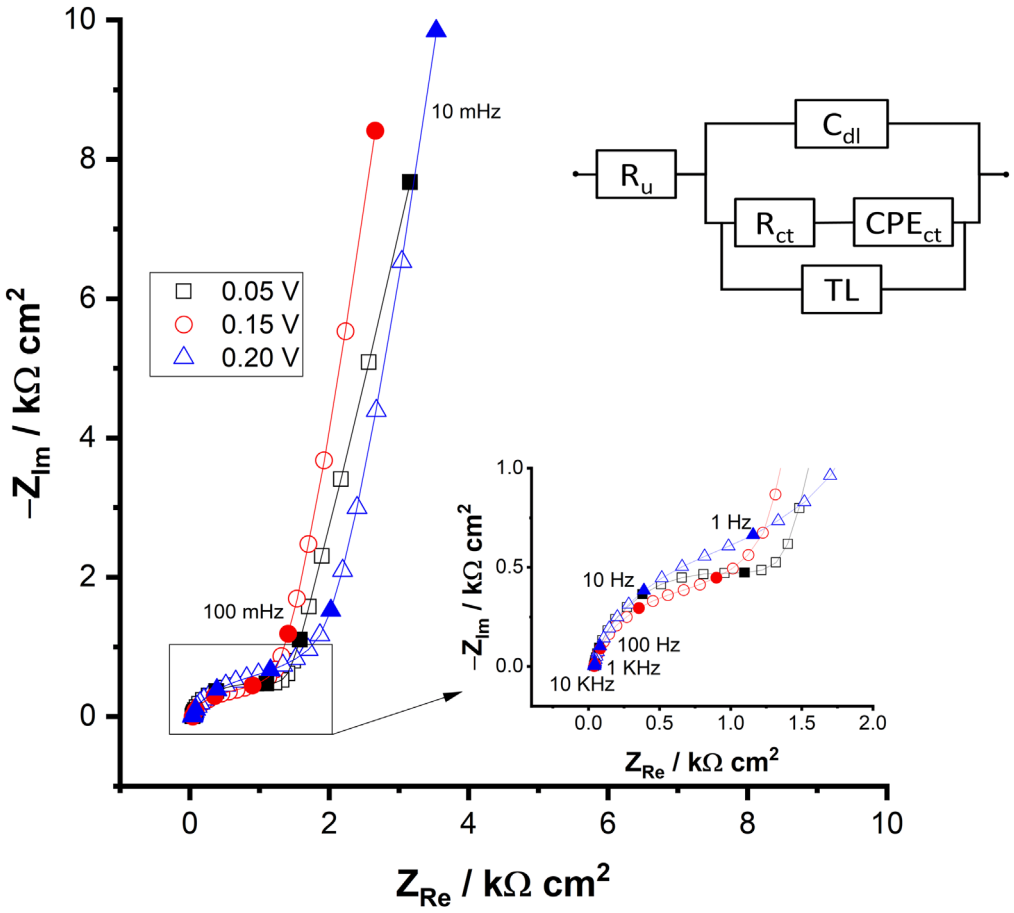

Figure 6. Nyquist plot including the equivalent circuit of PAA in 0.1 M acetate buffer (pH 3) and 0.45 M $NaNO_3$ at 0.05, 0.15 and 0.2 V between 10 mHz and 10 KHz with a potential amplitude 20 mV *rms*.

Table II. Impedance measurements from the fittings of impedance data with the equivalent circuit in Fig. 6.

E (V)	R_{ct} (kΩ cm^2)	CPE_{ct} (mF cm^{-2})	R_{tl} (kΩ cm^2)	C_{tl} (mF cm^{-2})
0.25	4.9	0.4	28.8	0.5
0.20	2.6	0.7	20.1	0.6
0.15	1.7	0.9	15.0	0.6
0.10	1.4	1.0	16.0	0.4
0.05	1.7	1.1	19.6	0.3

Figure 7b shows $CE^{EIS}_{R,G,B}$ at the studied potentials for the PAA films in terms of mol when this magnitude is multiplied by the Faraday constant (96485 C mol^{-1}). Coloration efficiency of the red color increases as phenothiazine rings are more electroactive at negatives potentials. The green color shows a maximum at 0.15 V, higher than the values of the red color at potentials more positives than 0.10 V. The blue color efficiencies confirm two different electrochemical processes associated with blue color changes as observed in the voltammetry of Fig. 2. It is important to note that DVEC has a high sensitivity to color changes since it can detect changes of 1 unit of intensity per nmol cm^{-2} of electrochromic centers.

One key advantage of DVEC is the spatiotemporal analysis of the electrode allowing the study of any area selected from the same experimental assay. Figure 7c shows the red color sinusoidal changes at 10 mHz for the more distant zone (straight line) and the closest zone (dotted line) to the electrical contact covered by Teflon. As observed, PAA shows a higher contrast in the distant zone than in the closest zone. This fact could be due to the non-homogeneous deposition of the film on the ITO electrode.[52] At the distant zone, PAA thickness could be thinner than at the closest zone caused by the ITO resistivity. Therefore, the contrast of the film depends on the film thickness. Besides, both signals show a small phase shift because the optical changes do not occur simultaneously due to the potential distribution along the electrode surface caused by the ITO resistivity.[52] The distant zone reaches the bleaching or colored state before the closest zone. These experimental proofs could explain the necessity of using a CPE_{ct} with $n_{ct} = 0.8$. DVEC can be a valuable technique to study electrochromic devices based on resistive electrodes like ITO.

Conclusions

PAA electrochromic changes in aqueous acidic media were investigated by DVEC. The new links formed during the polymerization and the heterocycles of phenothiazine rings have a noteworthy influence on the red, green, and blue components of the observed color. The green and red color intensities of the PAA are strongly modified by the heterocycle electrochemistry and weakly by the links between monomer units. The blue component is principally modified by the link electrochemistry between 0.5 V and −0.1 V. The PAA shows short optical response times. The bleaching process takes between 2.9 and 5.5 s depending on the applied potential and the analyzed color. The best coloration efficiencies were obtained for the green and red colors reaching values between 15–25 cm^2 mC^{-1}. Our results show the PAA as an attractive candidate for electrochromic devices compared with other electrochromic devices based on phenothiazines. From impedance measurements, it is possible to calculate coloration efficiencies at a given frequency with a

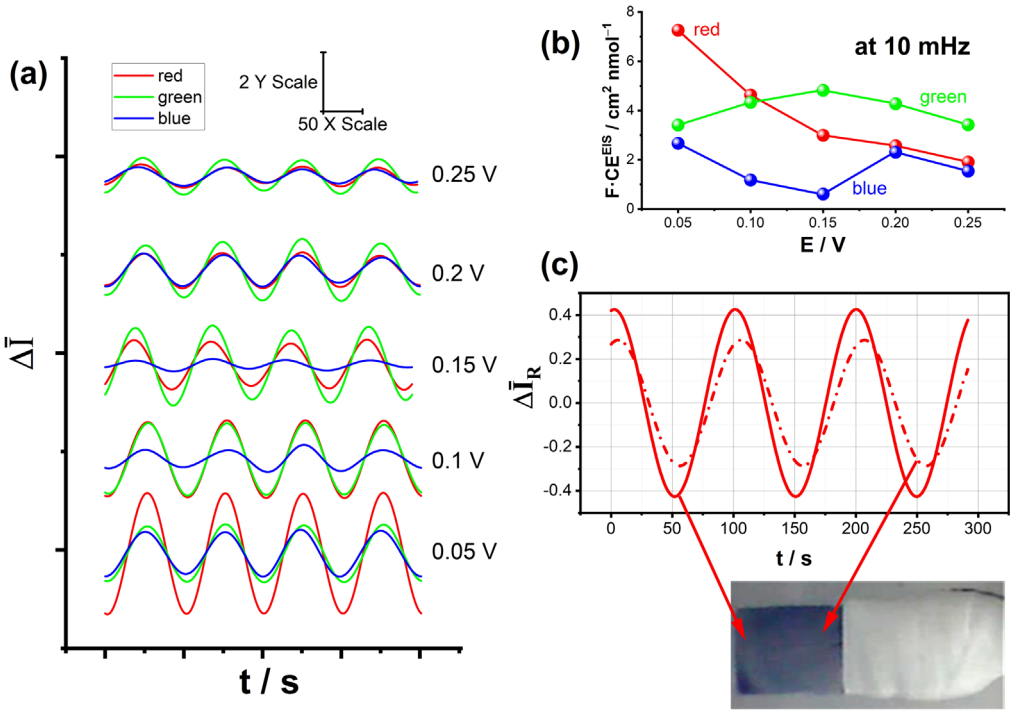

Figure 7. (a) Variation of R, G, and B mean color intensity at 0.25–0.05 V during the 10 mHz potential perturbation of PAA film in 0.1 M acetate buffer (pH 3) and 0.45 M $NaNO_3$. (b) Color efficiency (Eq. 13) in $cm^2\ nmol^{-1}$ for R, G and B colors between 0.25 and 0.05 V at 10 mHz. (c) Variation of mean color intensity of the red color at 10 mHz potential perturbation at two regions of the electrode surface.

sensitivity in the range of 1 unit of color intensity per nmol cm^{-2}. The spatiotemporal analysis of color in different zones and simultaneously allows characterizing the inhomogeneities of film deposition and the effect of the electrode resistivity on the color changes of PAA. In this work, DVEC is presented as a fast, non-expensive, accurate, and precise technical approach to the analysis of the electrochromic performance of films that can be extrapolated to mounted electrochromic devices. Our present work provides an important insight into the design principles for a practical application of DVEC to characterize electrochromic devices in light-controlled conditions allowing us to find the best performances.

Acknowledgments

This work was supported by MINECO-FEDER project CTQ2015-71794-R and CTQ2017-90659-REDT (MINECO, Spain).

ORCID

Esteban Guillén https://orcid.org/0000-0001-6837-2271
Jerónimo Agrisuelas https://orcid.org/0000-0003-0193-2857
José J. García-Jareño https://orcid.org/0000-0002-9247-1314
Francisco Vicente https://orcid.org/0000-0003-1628-918X

References

1. P. Monk, R. Mortimer, and D. Rosseinsky, *Electrochromism and Electrochromic Devices* (Cambridge University Press, United Kingdom) p. 511 (2007).
2. X. Li, K. Perera, J. He, A. Gumyusenge, and J. Mei, *J. Mater. Chem. C*, **7**, 12761 (2019).
3. C. G. Granqvist, M. A. Arvizu, İ. Bayrak Pehlivan, H.-Y. Qu, R.-T. Wen, and G. A. Niklasson, *Electrochim. Acta*, **259**, 1170 (2018).
4. I. Sorar, C. G. Granqvist, and G. A. Niklasson, *J. Electrochem. Soc.*, **167**, 026514 (2020).
5. P. M. Beaujuge and J. R. Reynolds, *Chem. Rev.*, **110**, 268 (2010).
6. S.-M. Chen and K.-C. Lin, *J. Electroanal. Chem.*, **511**, 101 (2001).
7. G. Inzelt and E. Csahók, *Electroanalysis*, **11**, 744 (1999).
8. U. Yogeswaran and S.-M. Chen, *J. Electrochem. Soc.*, **154**, E178 (2007).
9. J. Agrisuelas, M.-I. González-Sánchez, and E. Valero, *J. Electrochem. Soc.*, **164**, G1 (2017).
10. C. Chen, X. Hong, T. Xu, L. Lu, and Y. Gao, *J. Electrochem. Soc.*, **162**, G54 (2015).
11. S. A. Jenekhe, L. Lu, and M. M. Alam, *Macromolecules*, **34**, 7315 (2001).
12. S. Bhadra, D. Khastgir, N. K. Singha, and J. H. Lee, *Prog. Polym. Sci.*, **34**, 783 (2009).
13. Y. Huang, H. Li, Z. Wang, M. Zhu, Z. Pei, Q. Xue, Y. Huang, and C. Zhi, *Nano Energy*, **22**, 422 (2016).
14. C. Chen, X. Hong, T. Xu, A. Chen, L. Lu, and Y. Gao, *J. Electrochem. Soc.*, **162**, H699 (2015).
15. M. M. Rahman, N. S. Lopa, Y. J. Kim, D.-K. Choi, and J.-J. Lee, *J. Electrochem. Soc.*, **163**, B153 (2016).
16. M. P. R. Romero, R. E. Brito, A. Palma, M. R. Montoya, J. M. R. Mellado, and R. Rodríguez-Amaro, *J. Electrochem. Soc.*, **164**, B97 (2017).
17. Y. Liu, N. Song, Z. Ma, K. Zhou, Z. Gan, Y. Gao, S. Tang, and C. Chen, *Mater. Chem. Phys.*, **223**, 548 (2019).
18. B. Qu, Z. J. Chen, Y. L. Liu, H. Y. Cao, S. G. Xu, S. K. Cao, Z. H. Lan, Z. Y. Wang, and Q. H. Gong, *Journal of Physics D-Applied Physics*, **39**, 2680 (2006).
19. C. Chen, Z. Gan, C. Xu, L. Lu, Y. Liu, and Y. Gao, *Electrochim. Acta*, **252**, 226 (2017).
20. A. Romeiro, C. Gouveia-Caridade, and C. M. A. Brett, *Corrosion Sci*, **53**, 3970 (2011).
21. J. Agrisuelas, D. Ferrus, C. Gabrielli, J. J. García-Jareño, H. Perrot, O. Sel, and F. Vicente, *Russ. J. Electrochem.*, **52**, 1137 (2016).
22. K. Piwowar, A. Blacha-Grzechnik, and J. Zak, *J. Electrochem. Soc.*, **166**, G163 (2019).
23. Z. Gan, N. Song, H. Zhang, Z. Ma, Y. Wang, and C. Chen, *J. Electrochem. Soc.*, **167**, 085501 (2020).
24. C. Chen, T. Xu, A. Chen, L. Lu, and Y. Gao, *J. Electrochem. Soc.*, **163**, G159 (2016).
25. D. Shan, S. L. Mu, and B. W. Mao, *Electroanal.*, **13**, 493 (2001).
26. A. A. Karyakin, E. E. Karyakina, and H.-L. Schmidt, *Electroanalysis*, **11**, 149 (1999).
27. J. Agrisuelas, C. Gabrielli, J. J. García-Jareño, D. Gimenez-Romero, H. Perrot, and F. Vicente, *J. Phys. Chem. C*, **111**, 14230 (2007).
28. G. Broncová, T. V. Shishkanova, P. Matějka, R. Volf, and V. Král, *Anal. Chim. Acta*, **511**, 197 (2004).
29. T. Drnovšek and A. Perdih, *Dyes Pigm.*, **67**, 197 (2005).
30. J. Agrisuelas, D. Giménez-Romero, J. J. García-Jareño, and F. Vicente, *Electrochem. Commun.*, **8**, 549 (2006).
31. J. Agrisuelas, J. J. García-Jareño, D. Gimenez-Romero, and F. Vicente, *Electrochim. Acta*, **55**, 6128 (2010).
32. J. Agrisuelas, A. Cuenca, A. Frau, D. Ferrús, J. J. García-Jareño, R. Sanchis-Gual, and F. Vicente, *J. Electrochem. Soc.*, **164**, H593 (2017).
33. C. Zhou, J. Han, and R. Guo, *Macromolecules*, **42**, 1252 (2009).
34. S. H. Cho, H. J. Lee, Y. Ko, and S.-M. Park, *J. Phys. Chem. C*, **115**, 6545 (2011).
35. C. Benmouhoub, J. Agrisuelas, N. Benbrahim, F. Pillier, C. Gabrielli, A. Kadri, A. Pailleret, H. Perrot, and O. Sel, *Electrochim. Acta*, **145**, 270 (2014).
36. P. Deng, Y. Feng, and J. Fei, *J. Electroanal. Chem.*, **661**, 367 (2011).

37. C. Yang, J. Zhao, J. Xu, C. Hu, and S. Hu, *Int. J. Environ. An. Ch.*, **89**, 233 (2009).
38. Z. Peng, L. Guo, Z. Zhang, B. Tesche, T. Wilke, D. Ogermann, S. Hu, and K. Kleinermanns, *Langmuir*, **22**, 10915 (2006).
39. C. Mihali and N. Vaum, *Recent Advances in Plasticizers*, ed. M. Luqman (IntechOpen, United Kingdom) 125 (2012), https://intechopen.com/books/recent-advances-in-plasticizers/use-of-plasticizers-for-electrochemical-sensors (accessed December 5, 2019).
40. C. Gabrielli, J. J. Garcia-Jareño, M. Keddam, H. Perrot, and F. Vicente, *J. Phys. Chem. B*, **106**, 3192 (2002).
41. J. Agrisuelas, M.-I. González-Sánchez, B. Gómez-Monedero, and E. Valero, *Polymers*, **10**, 48 (2018).
42. A. A. Nekrasov, V. F. Ivanov, and A. V. Vannikov, *J. Electroanal. Chem.*, **482**, 11 (2000).
43. A. Kraft, *ChemTexts*, **5**, 1 (2018).
44. G. Y. Karaca, E. Eren, G. C. Cogal, E. Uygun, L. Oksuz, and A. Uygun Oksuz, *Opt. Mater.*, **88**, 472 (2019).
45. L. Ma, S. Xiao, N. Wu, S. Zhao, and D. Xiao, *Dyes Pigm.*, **168**, 327 (2019).
46. K. Su, N. Sun, X. Tian, S. Guo, Z. Yan, D. Wang, H. Zhou, X. Zhao, and C. Chen, *Dyes Pigm.*, **171**, 107668 (2019).
47. J. Agrisuelas, J. J. García-Jareño, E. Perianes, and F. Vicente, *Electrochem. Commun.*, **78**, 38 (2017).
48. R. J. Mortimer and T. S. Varley, *Dyes Pigm.*, **89**, 169 (2011).
49. J. Agrisuelas, J. J. García-Jareño, and F. Vicente, *Electrochim. Acta*, **269**, 350 (2018).
50. J. Agrisuelas, J. J. García-Jareño, and F. Vicente, *Electrochem. Commun.*, **93**, 86 (2018).
51. J. Agrisuelas, J. J. García-Jareño, E. Guillén, and F. Vicente, *Electrochim. Acta*, **305**, 72 (2019).
52. J. Agrisuelas, J. J. García-Jareño, and F. Vicente, *J. Electrochem. Soc.*, **165**, G101 (2018).
53. H. Zhang, Y. Zhai, and S. Dong, *Talanta*, **129**, 139 (2014).
54. C. Chen, X. Hong, T. Xu, J. Lu, and Y. Gao, *Synth. Met.*, **205**, 175 (2015).
55. C. Chen, Z. Gan, K. Zhou, Z. Ma, Y. Liu, and Y. Gao, *Electrochim. Acta*, **283**, 1649 (2018).
56. C. Chen and Y. Gao, *Electrochim. Acta*, **52**, 3143 (2007).
57. B. Gohain, S. Sarma, and R. K. Dutta, *J. Mol. Liq.*, **142**, 130 (2008).
58. M. Hepel and W. Janusz, *Electrochim. Acta*, **45**, 3785 (2000).
59. J. Agrisuelas, J. J. García-Jareño, E. Guillén, and F. Vicente, *J. Phys. Chem. C*, **124**, 2050 (2020).
60. J. Agrisuelas, C. Gabrielli, J. J. García-Jareño, H. Perrot, and F. Vicente, *J. Phys. Chem. C*, **115**, 11132 (2011).
61. D. Benito, C. Gabrielli, J. J. García-Jareño, M. Keddam, H. Perrot, and F. Vicente, *Electrochim. Acta*, **48**, 4039 (2003).
62. M. Gicevicius, J. Kucinski, A. Ramanaviciene, and A. Ramanavicius, *Dyes Pigm.*, **170**, 107457 (2019).
63. S. Hassab, D. E. Shen, A. M. Österholm, M. Da Rocha, G. Song, Y. Alesanco, A. Viñuales, A. Rougier, J. R. Reynolds, and J. Padilla, *Sol. Energy Mater. Sol. Cells*, **185**, 54 (2018).
64. H. Hu, L. Hechavarría, and J. Campos, *Solid State Ionics*, **161**, 165 (2003).
65. A. B. Atar, J. Y. Jeong, S. H. Han, and J. S. Park, *Polymer*, **153**, 95 (2018).
66. Y. C. Choi, R. S. Kumar, N. Mergu, J. Jeong, and Y.-A. Son, *Synth. Met.*, **240**, 1 (2018).
67. X. Ma, H. Niu, W. Cai, T. Xiao, C. Wang, X. Bai, Y. Zhang, and W. Wang, *React. Funct. Polym.*, **108**, 63 (2016).
68. E. N. Esmer, S. Tarkuc, Y. A. Udum, and L. Toppare, *Mater. Chem. Phys.*, **131**, 519 (2011).
69. E. K. Unver, S. Tarkuc, Y. A. Udum, C. Tanyeli, and L. Toppare, *J. Polym. Sci., Part A: Polym. Chem.*, **48**, 1714 (2010).
70. H.-J. Yen and G.-S. Liou, *J. Mater. Chem.*, **20**, 9886 (2010).
71. J. Agrisuelas, C. Gabrielli, J. J. García-Jareño, H. Perrot, R. Sanchis-Gual, O. Sel, and F. Vicente, *Electrochim. Acta*, **194**, 292 (2016).
72. J. J. García-Jareño, A. Sanmatías, J. Navarro-Laboulais, D. Benito, and F. Vicente, *Electrochim. Acta*, **43**, 235 (1998).